Environmental Science & Technology

pubs.acs.org/est

Article

Water-Driven Surface Lattice Oxygen Activation in MnO_2 for Promoted Low-Temperature NH_3−SCR

Dongqi An, Shan Yang, Qianni Cheng, Wanting Yan, Jingfang Sun,* Weixin Zou,* Chuanzhi Sun,* Changjin Tang, and Lin Dong

Cite This: *Environ. Sci. Technol.* 2024, 58, 16974−16983

Read Online

ACCESS | Metrics & More | Article Recommendations | Supporting Information

ABSTRACT: Water is ubiquitous in various heterogeneous catalytic reactions, where it can be easily adsorbed, chemically dissociated, and diffused on catalyst surfaces, inevitably influencing the catalytic process. However, the specific role of water in these reactions remains unclear. In this study, we innovatively propose that H_2O-driven surface lattice oxygen activation in γ-MnO_2 significantly enhances low-temperature NH_3−SCR. The proton from water dissociation activates the surface lattice oxygen in γ-MnO_2, giving rise to a doubling of catalytic activity (achieving 90% NO conversion at 100 °C) and remarkable stability. Comprehensive *in situ* characterizations and calculations reveal that spontaneous proton diffusion to the surface lattice oxygen reduces the orbital overlap between the protonated oxygen atom and its neighboring Mn atom. Consequently, the Mn−O bond is weakened and the surface lattice oxygen is effectively activated to provide excess oxygen vacancies available for converting O_2 into O_2^-. Therefore, the redox property of Mn−H is improved, leading to enhanced NH_3 oxidation-dehydrogenation and NO oxidation processes, which are crucial for low-temperature NH_3−SCR. This work provides a deeper understanding and fresh perspectives on the water promotion mechanism in low-temperature NO_x elimination.

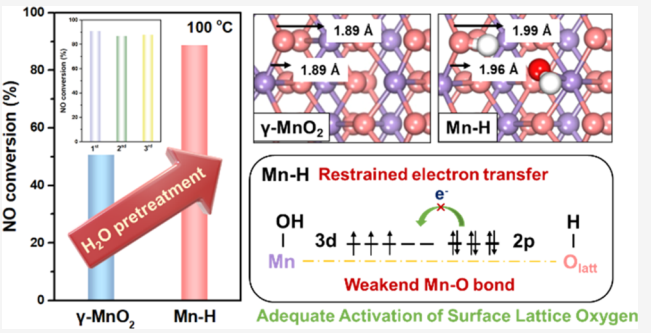

KEYWORDS: *NH_3−SCR, water-promoting effect, lattice oxygen activation, MnO_2, proton diffusion*

1. INTRODUCTION

NH_3−SCR technology is currently practiced in the elimination of nitrogen oxides in steel, cement, chemical, and other nonelectric industries.[1,2] H_2O, as an inherent component of low-temperature SCR, comes from both front-end wet desulfurization (the content is about 5−15%) and the reaction itself.[3,4] And due to the enhanced capillary condensation effect at low temperatures, H_2O forms a liquid film more easily on the catalyst surface, which to some extent exacerbates its toxic effect. Therefore, understanding the specific mechanism of H_2O in the reaction process, especially its impact on the catalyst structure, is not only quite beneficial for developing high-performance catalysts at low temperatures, but also of great meaning for improving the H_2O tolerance.

Generally, H_2O is believed to cause an unfavorable effect on most catalytic reactions, including the denitrification reaction, as it competes with reactants for available adsorption sites and also covers the active sites.[5,6] The conclusion is mainly based on the macroscopic effect of reduced catalytic activity caused by the introduction of H_2O. However, recent research into the reaction processes has led to a better understanding of the mechanism of H_2O. For example, numerous studies have reported on the positive effects of H_2O in catalytic reactions. Some works proposed that H_2O can enhance the catalytic reaction indirectly via the improvement of reactant adsorption and intermediate conversion. Bi et al. showed that H_2O was beneficial for the toluene adsorption on Pd supported on UiO-66 catalysts, resulting in the formation of benzoate and maleic acid intermediates in toluene oxidation.[7] Wei et al. proposed that the mechanism behind water-promoted alcohol oxidation lay in the enhanced adsorption of the reactant benzyl alcohol through hydrogen-bonding interactions with H_2O. This interaction reduced the intramolecular energy of benzyl alcohol, thereby facilitating its conversion.[8] Most notably, H_2O can interact with O_2 to facilitate oxygen activation or directly enhance catalytic reactions by utilizing its oxygen atom as an active oxygen. For example, our previous work indicated that O_2 could be synergistically activated by H_2O, with the water-induced reactive oxygen species counteracting SO_2 poisoning over Mn-based SCR catalysts.[9] In addition, CO molecules could react with the active hydroxyl groups from the

Received: June 23, 2024
Revised: August 25, 2024
Accepted: August 29, 2024
Published: September 9, 2024

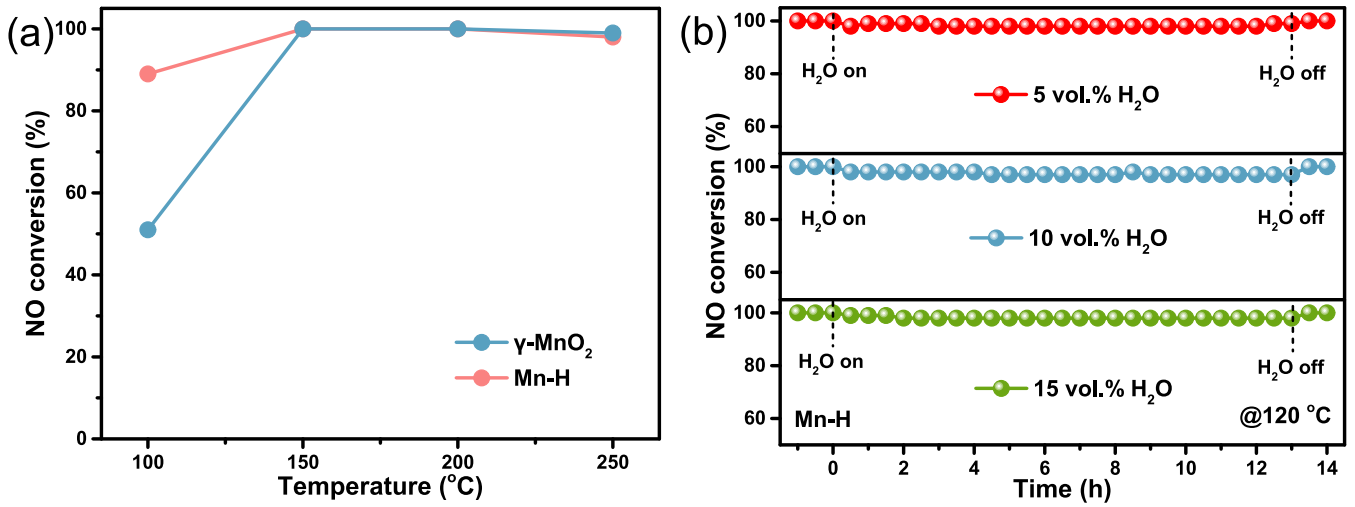

Figure 1. (a) Catalytic NO reduction performance of γ-MnO_2 and Mn−H. (b) H_2O tolerance over Mn−H under different H_2O contents at 120 °C (the feeding gas contained 500 ppm of NH_3, 500 ppm of NO, 5 vol % O_2, 5, 10, or 15 vol % H_2O (when used), and Ar balance, WHSV = 60,000 mL·g^{-1}·h^{-1}).

dissociation of H_2O on the surface of Au_1/CeO_2 or Pt_1/CeO_2, resulting in excellent oxidation activity.[10,11] On single Pt atoms catalysts, surface lattice oxygen activation by steam treatment has been an important reason for low-temperature CO oxidation.[12] Furthermore, the lattice oxygens of transition metal oxides also could be activated by H_2O, highlighting the role of water in the VOCs catalytic combustion.[13]

Excitingly, a novel promoting effect of H_2O has also been found in NH_3−SCR reaction, where H_2O changes the states of active centers in catalysts, affecting the catalytic reaction.[14−16] Ji et al. reported that the dissociation of H_2O on MnCe catalysts generated numerous hydroxyl groups, which limited charge transfer between active Mn sites and sulfur species, thereby hindering SO_2 oxidation. These findings highlight the positive effect of H_2O in SCR. However, research on this topic has mostly focused on adsorption and dissociation, particularly the impact of hydroxyl groups produced by H_2O dissociation. The effect of protons (with their high diffusion coefficients) on active centers of the SCR catalysts has rarely been addressed. Moreover, understanding this effect is complicated by the diverse components of catalysts, which might not be conducive to investigating the water-promoting mechanisms.

Herein, two SCR catalysts, γ-MnO_2 and steam-treated γ-MnO_2 (Mn−H), were constructed to explore the role of H_2O in a promoted NH_3−SCR process. Detailed characteristic analysis and density functional theory (DFT) calculations were adopted to study the influence on the catalytic performance of γ-MnO_2 by water in the catalytic reduction of NO, unraveling the specific process of water-driven surface lattice oxygen activation in the NH_3−SCR reaction.

2. MATERIALS AND METHODS

2.1. Catalyst Preparation. γ-MnO_2 was made via a hydrothermal approach. Initially, the same amounts of $MnSO_4 \cdot H_2O$ and $(NH_4)_2 \cdot S_2O_8$ were dissolved in deionized water and stirred continuously for 2 h to yield the resulting solution. Then, the solution was transferred into a stainless-steel autoclave and heated at 90 °C for 24 h. After cooling, the product was filtered, thoroughly washed, and dried overnight at 80 °C. The material was subsequently subjected to calcination in air at 350 °C for 3 h. This catalyst was labeled as γ-MnO_2.

Steam-treated γ-MnO_2 was produced by the steam treatment. 200 mg of γ-MnO_2 was preprocessed for 2 h in Ar flow with 5 vol % H_2O introduced (200 mL·min^{-1}) at the temperature of 100, 150, 200, and 250 °C, respectively. The obtained sample was labeled Mn−H (-T).

2.2. Characterization and Performance Measurements. Detailed characterization methods (XRD, N_2 adsorption−desorption, Raman, H_2-TPR, XPS, TPD, EPR, Py-IR, *in situ* DRIFTS and computational details) and performance measurements (SCR performance measurements and kinetics measurements) are provided in the Supporting Information (SI).

3. RESULTS AND DISCUSSION

3.1. NH_3−SCR Performance. The NO conversion curves were measured to evaluate catalytic performance in the temperature range of 100−250 °C. As shown in Figure 1a, 100% denitrification efficiency was achieved at 150−250 °C over γ-MnO_2, demonstrating that γ-MnO_2 was a promising catalyst for low-temperature NO removal.[17,18] After steam treatment, Mn−H exhibited dramatically improved reactivity at 100 °C compared to that of γ-MnO_2, as the NO conversion rose to approximately 90% from 51%. Furthermore, no noticeable deactivation was detected during the stability test with three cycles (Figure S1). In addition, the NO conversion of steam-treated γ-MnO_2 at different temperatures was measured as well. As displayed in Figure S2, the catalysts with steam treatment presented elevated catalytic activity, and the difference in NO conversion of the four Mn−H samples was only 10%, indicating that the catalytic performances would not be significantly affected by the pretreatment temperatures, and the temperature of 250 °C was chosen for investigation. There was no obvious change in N_2 selectivity before and after steam treatment, and the slight improvement may be due to the inhibition of byproduct N_2O formation by H_2O (Figure S3).[14]

To investigate the interference of vapor on Mn−H catalyst, stability tests over catalyst were conducted under different H_2O contents at 120 °C. As revealed by Figure 1b, when H_2O

https://doi.org/10.1021/acs.est.4c06313
Environ. Sci. Technol. 2024, 58, 16974−16983

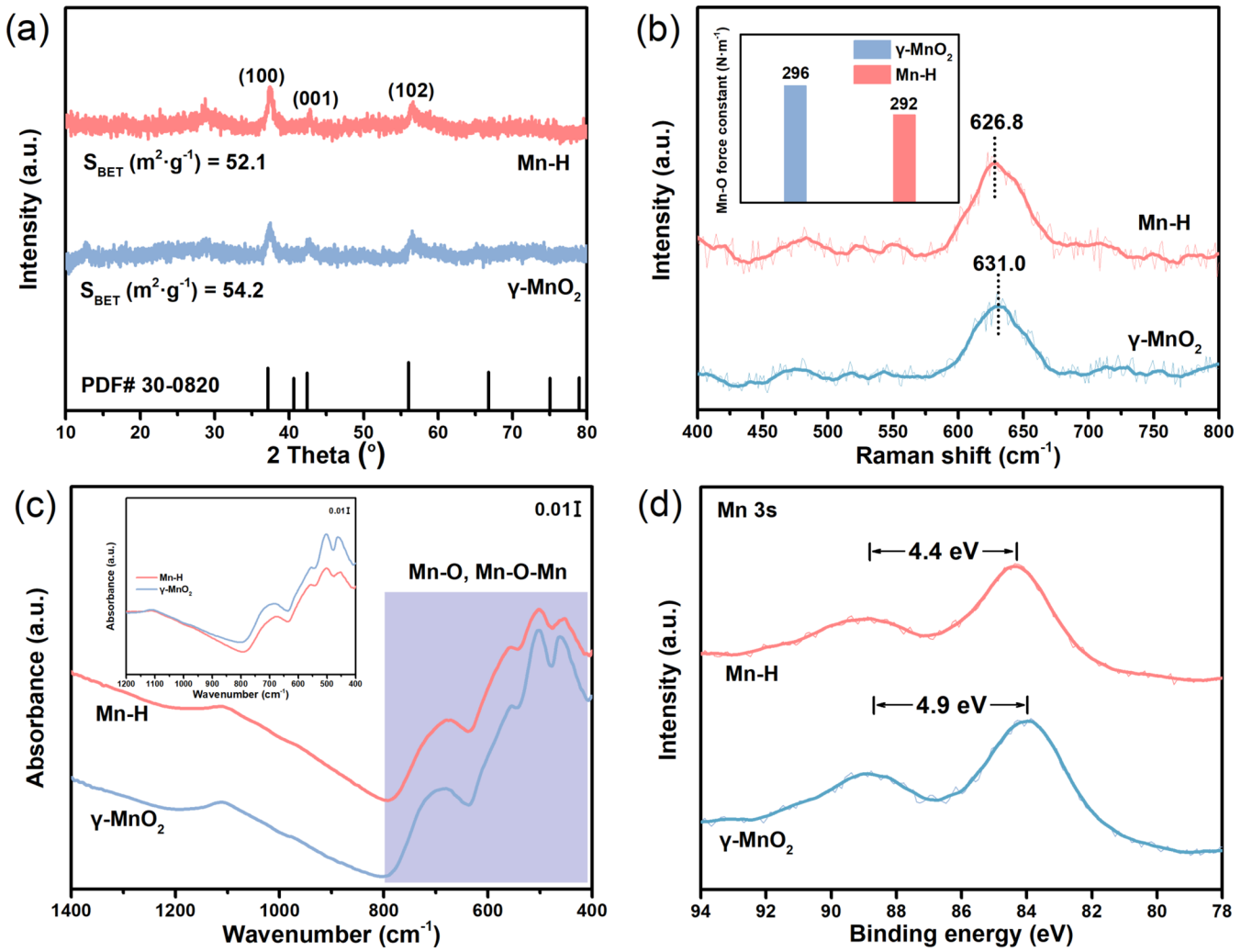

Figure 2. (a) XRD patterns and BET surface area; (b) Raman spectra and the corresponding force constant of the Mn−O bond; (c) FT-IR spectra (inset: spectra with the baselines overlapped); and (d) XPS patterns of Mn 3s of γ-MnO_2 and Mn−H.

was introduced into the reaction condition, only an invisible drop in NO conversion over Mn−H after 12 h appeared, even though the H_2O content reached up to 15 vol %. It indicated that the resistance to H_2O of Mn−H was quite superior. When H_2O was withdrawn from the reaction condition, the NO conversion returned to its original level at once, suggesting that the declining activity resulted from competition adsorption between the reactants and H_2O on the active sites of the catalyst.

Therefore, H_2O-activation-γ-MnO_2 (Mn−H) was provided with the promoted low-temperature NH_3−SCR. Compared with γ-MnO_2, Mn−H showed about double the performance improvement at 100 °C in the NH_3−SCR reaction. Comprehensive *in situ* characterizations and calculations were further implemented to explore the water promotion effect.

3.2. H_2O-Weakened Mn−O Bond. To determine any interaction between water and the catalyst, detailed characterizations were employed accordingly. XRD patterns of γ-MnO_2 are displayed in Figure 2a, in which the diffraction peaks corresponded to the (100), (001), and (102) planes (PDF# 30-0820).[19] Mn−H, the sample treated with steam, could retain the original structure. Additionally, the specific surface areas between the two catalysts hardly changed (54.2 and 52.1 $m^2 \cdot g^{-1}$), indicating that the steam treatment had little effect on the textural properties.

The Raman characterization was used to analyze the bonding properties. In Figure 2b, the peak at 631.0 cm^{-1} attributed to the Mn−O stretching vibration in γ-MnO_2 was observed,[20] which became a visible broadening at around 626.8 cm^{-1} after the steam treatment for the Mn−H sample, suggesting that the crystallinity was decreased and more defects were generated, possibly due to the lattice distortion.[21,22] In addition, the bond strength of Mn−O was calculated using Hooke's law. The equation is as follows[21]

$$\omega = \frac{1}{2\pi c}\sqrt{\frac{k}{\mu}}$$

where k is the bond force constant, ω is the Raman shift of the stretching vibration of the Mn−O bond, μ is the Mn−O bond effective mass, and c is the velocity of light. It could be observed that there was a certain red shift (from 631.0 to 626.8 cm^{-1}) coming from the Mn−O bond after the steam treatment, which resulted in the weaker bond energy of Mn−H (292 $N \cdot m^{-1}$), compared to that of γ-MnO_2 (296 $N \cdot m^{-1}$). In a previous report, it was proposed that the rupture of the unsaturated metal−oxygen bond led to the lattice oxygen desorption on surface (O_β).[23] Based on this, it was suggested

https://doi.org/10.1021/acs.est.4c06313
Environ. Sci. Technol. 2024, 58, 16974−16983

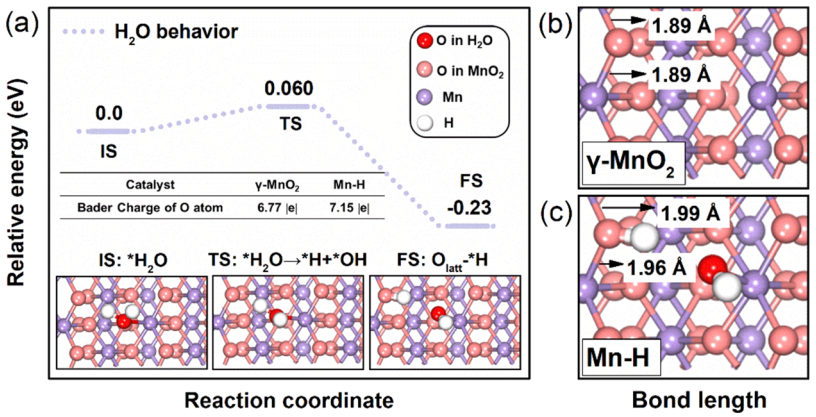

Figure 3. (a) Optimized configurations and energy profiles for the H_2O behavior on γ-MnO_2 (100) surface; insets show the Bader charge of O atom before and after protonation. Length of the Mn−O bond from (b) γ-MnO_2 and (c) Mn−H. Color code: purple, Mn; red, O in H_2O; pink, O in MnO_2; white, H.

that the Mn−H sample was provided with a weakened bond, which resulted in enhanced redox properties and thus improved catalytic performance. Moreover, the FT-IR characterization was carried out on the γ-MnO_2 and Mn−H samples (Figure 2c). The absorption bands at 800−400 cm^{-1} were detected, which were the metal−oxygen vibrations in the octahedron of the [MnO_6] type of MnO_2.[24] On the Mn−H sample after the steam treatment, the peak intensity was decreased, which was related to the breakage of the Mn−O bond in MnO_2,[25] confirmed by the Raman results.

Further, XPS technology was also adopted to study the valence states of the catalysts on the surface. Generally, based on the following equation, the average oxidation state (AOS) of Mn species has a linear relationship with the multiplet splitting of Mn 3s[26]

$$\mathrm{AOS} = 8.95 - 1.13 \times \Delta E_{\mathrm{Mn\ 3s}}$$

In Figure 2d, the multiplet splitting values of γ-MnO_2 and Mn−H samples were 4.9 and 4.4 eV, respectively, from which the AOS was calculated to be 3.41 for γ-MnO_2 and 3.98 for Mn−H. The relative percentage of Mn^{4+} derived from Mn 2p also well corroborated the above conclusion (from 50.5 to 55.5%) (Figure S4). Meanwhile, a higher chemical shift was observed in Mn^{4+} of Mn−H. In general, the shifted energies of the emitted photoelectrons were related to the changed chemical states.[27] The density of the electrons around the atom became higher, and thus the E_K of photoelectrons from its core levels was higher, leading to lower E_B chemical shift in the XPS spectrum ("E_K" refers to the kinetic energy of photoelectrons excited by incident photons, and "E_B" refers to the orbital binding energy of inner electrons).[28] It indicated that there was an increase in the average valence state in Mn species and a decrease in the electron cloud density around Mn atoms induced by water.

3.3. Activation Mechanism of Surface Lattice Oxygen.

DFT calculations were employed to further explore the mechanism of the water-induced effect. The behaviors of water are illustrated in Figure 3a, through the highly exposed (100) facets of γ-MnO_2 according to our previous work.[9] Initially, the O atom (H_2O molecule) was bonded to the Mn atom (γ-MnO_2) to form a stable adsorption configuration (IS). Then, the dissociation of H_2O molecule into proton and hydroxyl was achieved, according to the report that the proton derived from water dissociation has anomalously large diffusion coefficients and can easily penetrate the oxide lattice and occupy interstitial positions.[29] The dissociated proton spontaneously diffused through the oxide lattice and freely migrated to the surface lattice oxygen to protonate it (FS), due to a quite low energy barrier (just 0.06 eV). Meanwhile, with the protonation of this O atom, the length of adjacent Mn−O bond was extended to 1.99 or 1.96 from 1.89 Å (Figure 3b,c), and the Bader charge indicated that more electrons were localized to the protonated O atom (inset in Figure 3a), weakening the Mn−O bond. In addition, the reduced orbital overlap between the protonated oxygen atom and the adjacent manganese atom would prevent the transfer process of electrons from the O 2p to the empty orbital of Mn 3d.[13] According to the results in Raman and FT-IR, lattice oxygen activation on the surface was aided by the weakened Mn−O bond. Therefore, the H_2O molecule promoted the spontaneous proton diffusion, and thus, the protonation of the lattice oxygen on the surface drove the activation process.

The ability of water-activated surface lattice oxygen could improve the redox abilities, reflected by the H_2-TPR technology (Figure 4a). Generally, two peaks were associated with the process of the reduction of $Mn^{4+} \rightarrow Mn^{4+}/Mn^{3+} \rightarrow Mn^{2+}$, respectively.[30] As a whole, the reduction process of H_2 on manganese dioxide could also be regarded as $Mn^{4+} + O_{latt}^{2-} + H_2 \rightarrow Mn^{2+} + H_2O$.[13] Compared with γ-MnO_2, it was easier for Mn−H to be reduced at a lower temperature (from 367 to 321 °C), meaning an enhanced redox process. More hydrogen consumption (0.085 mmol·g^{-1}) was observed on Mn−H than γ-MnO_2 (0.075 mmol·g^{-1}), demonstrating the larger amount of Mn^{4+}, which was in accordance with the results from XPS analysis. Accordingly, Mn−H had a stronger redox property with the aid of water-driven activation.

Generally, the excellent redox capacity from the reactive oxygen species is important to low-temperature SCR reaction, and thus O_2-TPD characterization was operated to further investigate the oxygen species after steam treatment (Figure 4b). The first region below 400 °C corresponded to surface adsorbed oxygen species at vacancy sites (O_2^-, O^-), and the second and third regions at 400−500 °C are ascribed to surface lattice oxygen species (surface O_{latt}^{2-}), respectively.[31] The desorption of surface O_{latt}^{2-} in Mn−H (75.2%) was significantly increased compared with γ-MnO_2 (60.5%) (inset in Figure 4b), indicating enhancement of lattice oxygen mobility in the Mn−H catalyst. This could be due to the

https://doi.org/10.1021/acs.est.4c06313
Environ. Sci. Technol. 2024, 58, 16974−16983

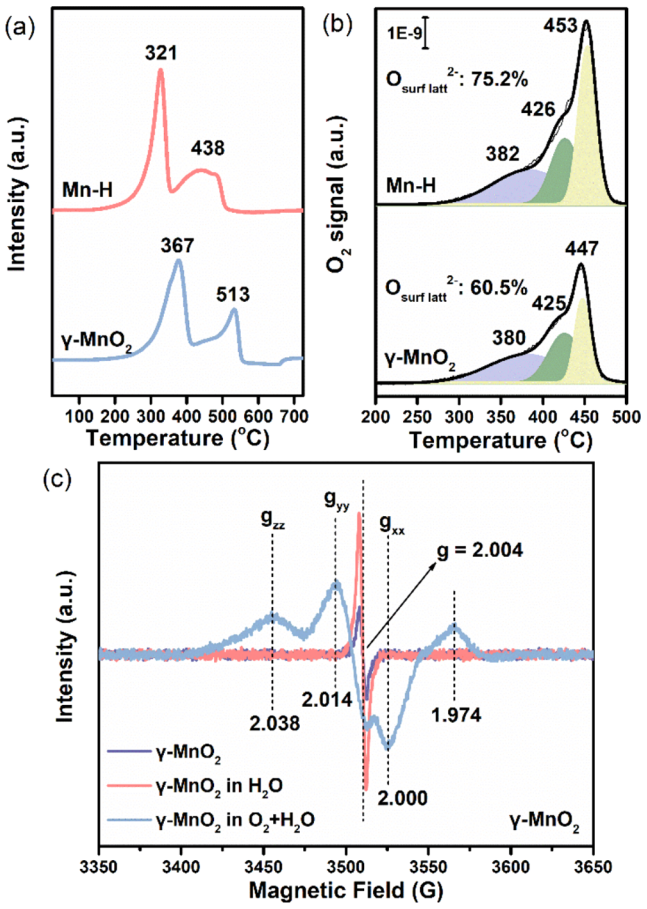

Figure 4. (a) H_2-TPR results, and (b) O_2-TPD profiles of γ-MnO_2 and Mn−H. (c) *In situ* EPR spectra over γ-MnO_2 collected in a flow of H_2O or O_2+H_2O.

weakening of the Mn−O bond[32] and the protonation of lattice oxygen increasing lattice distortion, as we analyzed in Raman, FT-IR, and DFT calculations. Therefore, the increased redox capability and low-temperature activity of Mn−H resulted from lattice oxygen activation on the surface, which may be a key factor.

To further identify the generated active species in the process of H_2O-induced surface lattice oxygen activation, the EPR spectra were collected in different atmosphere conditions (Figure 4c). After γ-MnO_2 stabilized in a flow of H_2O, the signal at g = 2.004 ascribed to the oxygen vacancy due to the electron capture on the oxygen defect[33] on the γ-MnO_2 was increased, which suggested that the occurrence of vapor boosted the oxygen vacancy formation. Therefore, richer vacancies in γ-MnO_2 were generated with the vapor activation surface lattice oxygen. Subsequently, the O_2 was added into the flow, and new signals emerged, where a signal located at around 1.974 was assigned to surface electron trapping sites related to the oxygen species,[34,35] and a group of signals (g_{xx} = 2.000, g_{yy} = 2.014, and g_{zz} = 2.038) were assigned to the paramagnetic superoxide O_2^- species.[33,36] The emerged signals suggested the activation of O_2 at oxygen vacancies from the H_2O pretreatment, bringing about an increase in active oxygen. In general, O_2^- is crucial in the NH_3−SCR process, as it can participate in the activation of reactant molecules and assist in the catalytic redox cycle. Generally, the O_2^- on the catalyst surface originates from the O_2 activation at the vacancies.[37] And according to the *in situ* EPR under the conditions of H_2O or O_2 + H_2O (Figure S5a and Figure S5b), it was found that with the pretreatment time, the effect of the vapor was to create more vacancies by the lattice oxygen activation on the surface, resulting in the increased oxygen species. The content of these generated reactive oxygen species under the O_2 + H_2O condition was much higher than that in only O_2 on γ-MnO_2, suggesting the superior ability of H_2O for the lattice oxygen activation on the surface.

3.4. Activation Process of Reactants. For the low-temperature denitrification, the excellent activation ability of reactant molecules was important to the catalytic performance due to lower energy consumption. Therefore, the effect of water-driven surface lattice oxygen activation on the activation of NH_3 and NO reactants was worth taking into account. Generally, the surface acidity is closely related to the NH_3 activation, and thus the surface acidity was determined by the NH_3-TPD technology (Figure S6a). The desorption peaks of NH_3 were mainly located below 300 °C, corresponding to the weak acid sites.[21] Notably, the total acidity of Mn−H dramatically increased compared to the original γ-MnO_2. Furthermore, the pyridine adsorption FT-IR spectra (Py-IR) were used to analyze the acidity information (Brønsted and Lewis). In Figure 5a, the peaks at ca. 1612, 1595, 1581, and 1444 cm^{-1} were attributed to the Lewis acid binding to the pyridine, and the Brønsted acid was found at the peaks at ca. 1643 and 1540 cm^{-1}, while the peak for either Lewis or Brønsted acid was at 1490 cm^{-1}.[38] It was found that for Mn−H, both acid sites were increased, which was consistent with the results in the NH_3-TPD profiles. Furthermore, the normalized peak areas at 1540 and 1444 cm^{-1} after desorption at 100 °C (Figure 5b) were used for the calculation of the amounts of Brønsted and Lewis acids. Apparently, on γ-MnO_2 and Mn−H, the Lewis acid sites were predominantly present, with a small content of Brønsted acid. In general, Brønsted acid came from hydroxyl groups and lattice oxygen protonation by water dissociation on the surface,[39] while Lewis acid resulted from Mn species with higher average states, which was provided with a stronger ability to accept electron pairs. But for NO, the nitrates adsorbed on Mn−H were much less than those on γ-MnO_2 (Figure S6b). It suggested that the adsorption of NO+O_2 on Mn−H was restrained by surface lattice oxygen protonation due to the competition adsorption.

Although surface acid modification is in favor of the improved catalytic performance, the activation of NH_3 and NO greatly depends on the redox performance at low temperatures.[40,41] The lattice oxygen on the surface from SCR catalyst participated in the conversion of NH_3 to NH_2 or NO to NO_2, crucial reactive intermediates involved in the reaction.[32] N_2O signal from the NH_3-TPD process can be employed to evaluate the level of NH_3 activation (Figure 5c) since N_2O is identified with the product of the overoxidation of NH_3 in an excess of active oxygen.[42,43] As expected, a stronger N_2O signal response appeared on Mn−H, signifying that its surface lattice oxygen was more active and its ability to activate NH_3 was stronger, compared with γ-MnO_2. In addition, the fast SCR reaction rate was 1−2 orders higher than the standard SCR reaction at low temperatures, effectively enhancing the denitrification performance, where the rate-determining step is oxidizing NO to NO_2. Therefore, the increase in NO_2 yield by the oxidation ability is an effective means to promote fast SCR reaction.[44,45] Here, the NO oxidation ability of the two catalysts was also evaluated (Figure 5d). Although the NO adsorption was largely inhibited over

https://doi.org/10.1021/acs.est.4c06313
Environ. Sci. Technol. 2024, 58, 16974−16983

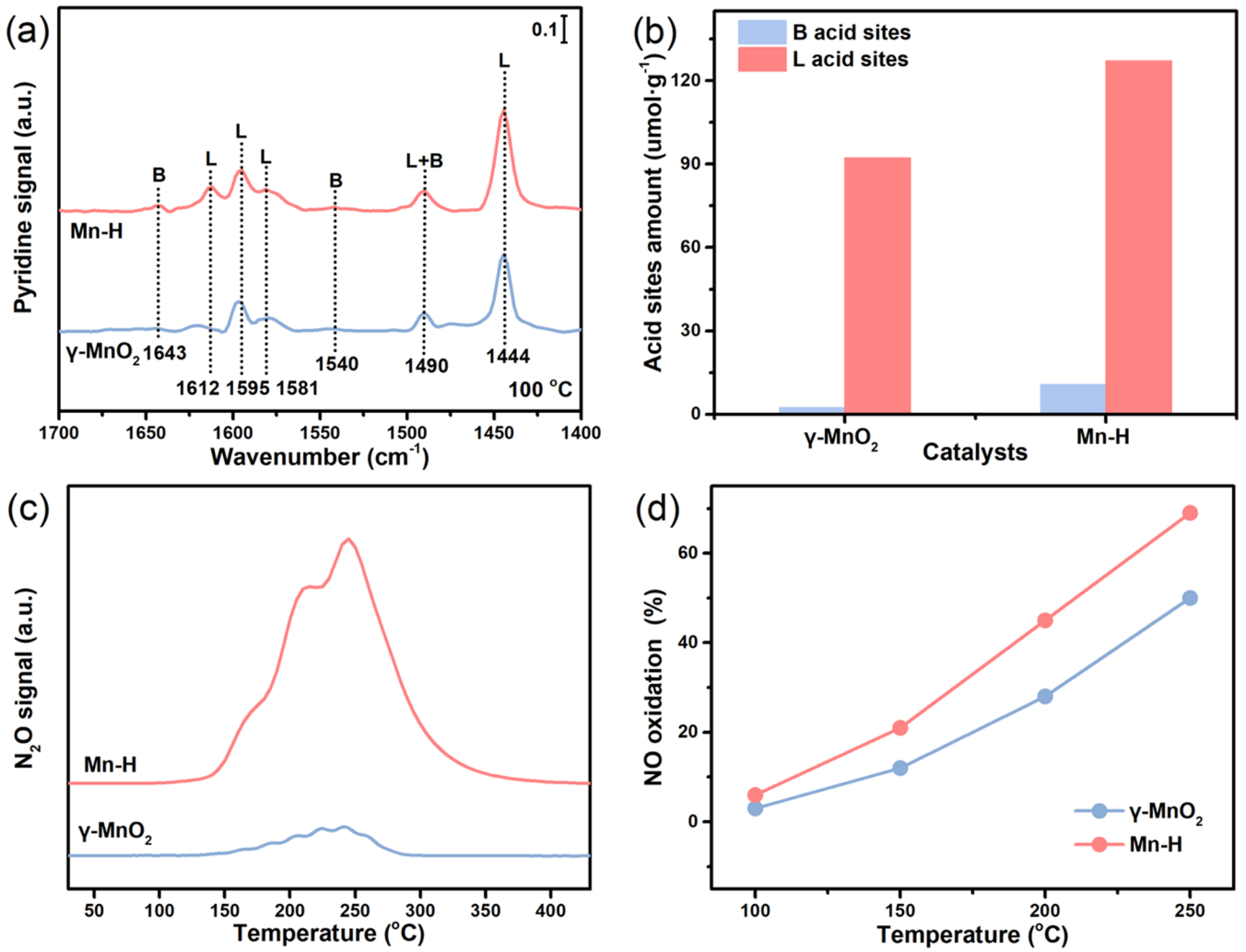

Figure 5. (a) Py-IR spectra, (b) acid sites amount (umol·g^{-1}) from the IR spectra of Py adsorption, (c) N_2O signal from NH_3-TPD results, and (d) NO oxidation ability of γ-MnO_2 and Mn−H.

Mn−H, its ability to oxidize NO unexpectedly upgraded throughout the entire reaction temperature. On the whole, the activation of reactant molecules (NH_3 and NO) was well promoted on Mn−H, facilitated by the Lewis acid sites (from higher average state of Mn) and excellent redox property, resulting from the active surface lattice oxygen.

3.5. Catalytic Mechanism. The kinetic study was also determined, with the purpose of further evaluating the catalytic mechanism. According to the calculation of the apparent energy of activation (E_a), the Arrhenius plots (Figure 6) showed that the E_a value of Mn−H was 25.8 kJ·mol^{-1}, which was lower than that of γ-MnO_2 (29.8 kJ·mol^{-1}). A lower E_a implied that the rate-determining step could proceed with less energy consumption in thermodynamics, which was in accordance with the promoted catalytic performance at low temperatures, proving that the process of water-driven surface lattice oxygen activation lowered the reaction energy barrier.

In situ DRIFTS characterization was conducted to acquire a deeper insight into the reaction mechanism on the γ-MnO_2 and Mn−H samples. The samples were preadsorbed with NH_3, and then the spectra of NO + O_2 at 150 °C on both catalysts are determined in Figure 7a,b, respectively. As for γ-MnO_2, the signals of Lewis acid (1267 and 1205 cm^{-1}) and Brønsted acid (1444 cm^{-1}) appeared.[46] When the NO and O_2 conditions

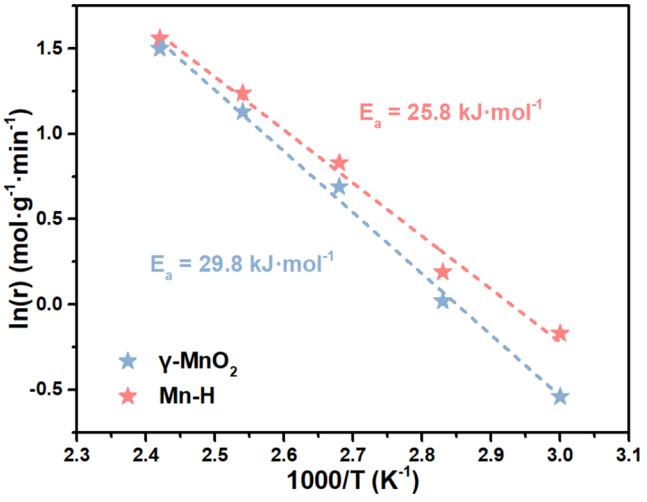

Figure 6. Arrhenius plots of γ-MnO_2 and Mn−H.

were introduced, the adsorbed NH_3 species reacted in less than 20 min, and the bridged and monodentate nitrates (1635, 1540, and 1284 cm^{-1}) began to accumulate.[47] Similarly, the Lewis acid with the bands at 1269 cm^{-1} and Brønsted acid (1458 and 1375 cm^{-1}) were detected on Mn−H after being

https://doi.org/10.1021/acs.est.4c06313
Environ. Sci. Technol. 2024, 58, 16974−16983

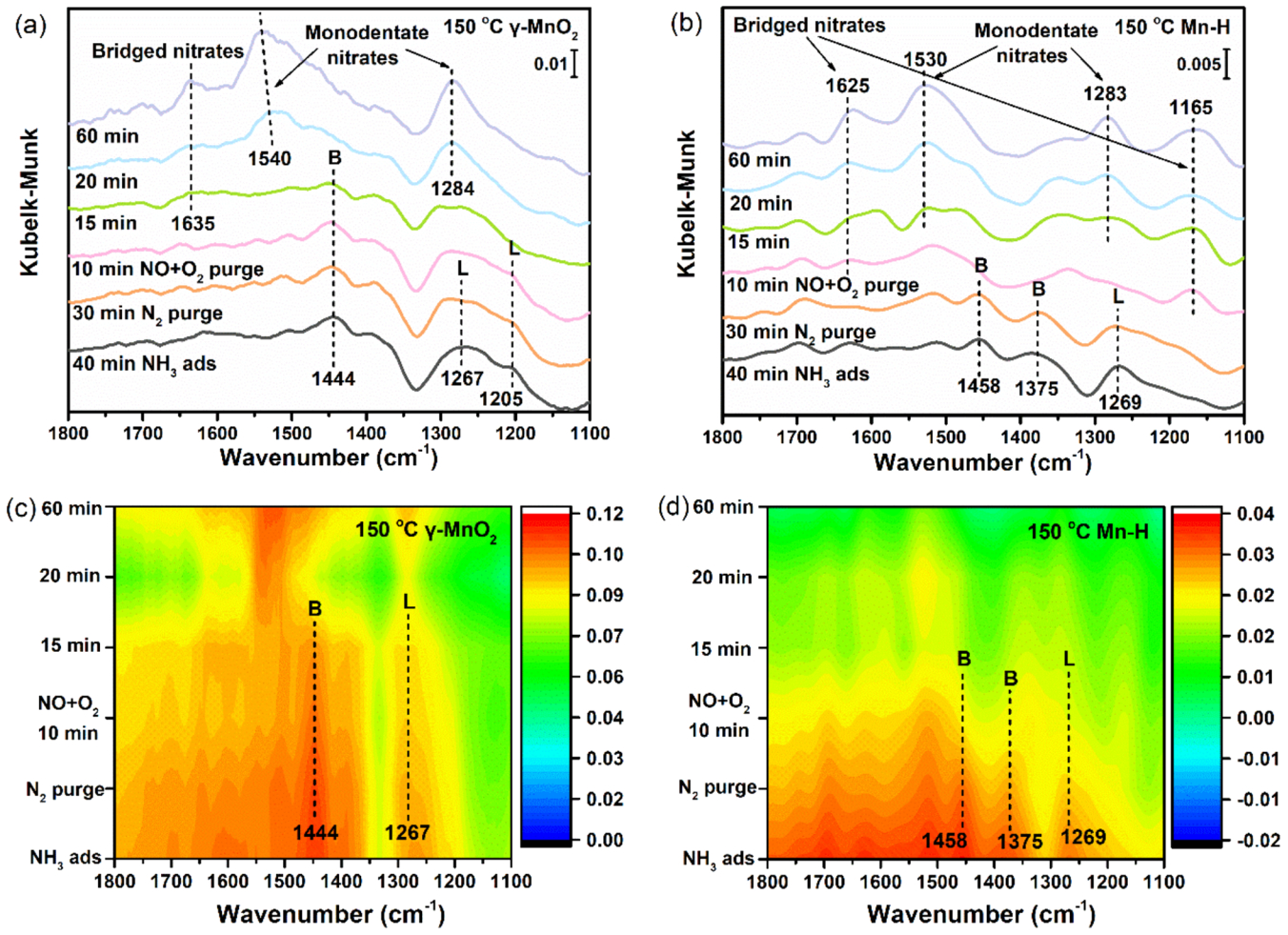

Figure 7. *In situ* DRIFTS spectra of NH_3 preabsorption and then NO + O_2 introduced over (a) γ-MnO_2 and (b) Mn−H. The acid sites on the catalyst surfaces of γ-MnO_2 and Mn−H as a function of reaction time relative to the initial infrared peak area for (c) Brønsted and (d) Lewis acid sites.

saturated with NH_3. Compared with the γ-MnO_2, NH_3 species adsorbed on Mn−H were completely reacted with NO + O_2 almost within 10 min, manifesting that NH_3 species were more well activated. Then, it was found that the bridged and monodentate nitrates (1625 and 1165 cm^{-1}, 1530 and 1283 cm^{-1}) appeared, respectively.

To determine the reaction rate of the adsorption of NH_3 on Lewis and Brønsted acid in NO + O_2 flow, the spectra were plotted in another clear form after subtracting the baseline (Figure 7**c**,**d**). Obviously, the consumption rate of NH_3 species on Mn−H was much higher than that on γ-MnO_2, both on Brønsted and Lewis acids, almost completely consumed within 10 min, showing the higher activity of NH_3 species over Mn−H. In addition, once the NO + O_2 was in the reaction condition, compared with the NH_3 species on Brønsted acid, the depleted NH_3 species on the Lewis acid of Mn−H was faster, which demonstrated that H_2O activation surface lattice oxygen generated abundant manganese ions with higher oxidation states, acting as Lewis acid sites to activate NH_3 molecules to improve the reaction performance. This strategy of the water-promoting effect was also adaptable to other metal oxide SCR catalysts. For example, CeO_2 as another common SCR catalyst was evaluated, and the sample pretreated by H_2O was denoted as Ce−H. In Figure S7, it was found that the Ce−H exhibits a significantly improved activity in a medium-temperature reaction.

4. ENVIRONMENTAL IMPLICATIONS

Elucidating the intrinsic mechanism behind the "transition from inhibition to promotion" by H_2O, and understanding how to fully exploit this promoting effect, is of great significance for designing and developing NH_3−SCR catalysts. This work investigates the influence of water on catalytic performance at low temperatures by using the common MnO_2 catalyst. The Mn−H catalyst demonstrated a 90% NO removal efficiency at 100 °C, with protons from water dissociation effectively activating surface lattice oxygen. This activation created more oxygen vacancies, which could be used to produce O_2^- from oxygen molecules. These processes facilitated better activation of NH_3 and NO, thereby enhancing the catalyst performance. Additionally, Mn−H exhibited excellent stability, with no observed performance decline even after three cycles, and showed strong resistance to H_2O. This research on water-driven surface lattice oxygen activation provides new insights for designing low-temperature NH_3−SCR catalysts.

https://doi.org/10.1021/acs.est.4c06313
Environ. Sci. Technol. 2024, 58, 16974−16983

■ ASSOCIATED CONTENT

Supporting Information

The Supporting Information is available free of charge at https://pubs.acs.org/doi/10.1021/acs.est.4c06313.

More details about the characterization methods (Text S1); cycling stability (Figure S1); NO conversion (Figure S2); N_2 selectivity (Figure S3); XPS patterns of Mn 2p (Figure S4); EPR spectra (Figure S5); NH_3-TPD and NO-TPD profiles (Figure S6); and NO conversion (Figure S7) (PDF)

■ AUTHOR INFORMATION

Corresponding Authors

Jingfang Sun − *Jiangsu Key Laboratory of Vehicle Emissions Control, Center of Modern Analysis, State Key Laboratory of Pollution Control and Resource Reuse, School of Environment, Key Laboratory of Mesoscopic Chemistry of MOE, School of Chemistry and Chemical Engineering, Nanjing University, Nanjing 210093, P. R. China;* orcid.org/0000-0003-1963-4874; Email: sunjf@nju.edu.cn

Weixin Zou − *Jiangsu Key Laboratory of Vehicle Emissions Control, Center of Modern Analysis, State Key Laboratory of Pollution Control and Resource Reuse, School of Environment, Key Laboratory of Mesoscopic Chemistry of MOE, School of Chemistry and Chemical Engineering, Nanjing University, Nanjing 210093, P. R. China;* orcid.org/0000-0001-5001-2841; Email: wxzou2016@nju.edu.cn

Chuanzhi Sun − *Collaborative Innovation Center of Functionalized Probes for Chemical Imaging in Universities of Shandong, Shandong Provincial Key Laboratory of Clean Production of Fine Chemicals, College of Chemistry, Chemical Engineering and Materials Science, Shandong Normal University, Jinan 250014, P. R. China;* orcid.org/0000-0002-3744-9800; Email: suncz@sdnu.edu.cn

Authors

Dongqi An − *Jiangsu Key Laboratory of Vehicle Emissions Control, Center of Modern Analysis, State Key Laboratory of Pollution Control and Resource Reuse, School of Environment, Key Laboratory of Mesoscopic Chemistry of MOE, School of Chemistry and Chemical Engineering, Nanjing University, Nanjing 210093, P. R. China; Sinopec (Beijing) Research Institute of Chemical Industry Co., Ltd., Beijing 100013, P. R. China*

Shan Yang − *Collaborative Innovation Center of Functionalized Probes for Chemical Imaging in Universities of Shandong, Shandong Provincial Key Laboratory of Clean Production of Fine Chemicals, College of Chemistry, Chemical Engineering and Materials Science, Shandong Normal University, Jinan 250014, P. R. China*

Qianni Cheng − *Jiangsu Key Laboratory of Vehicle Emissions Control, Center of Modern Analysis, State Key Laboratory of Pollution Control and Resource Reuse, School of Environment, Key Laboratory of Mesoscopic Chemistry of MOE, School of Chemistry and Chemical Engineering, Nanjing University, Nanjing 210093, P. R. China*

Wanting Yan − *Jiangsu Key Laboratory of Vehicle Emissions Control, Center of Modern Analysis, State Key Laboratory of Pollution Control and Resource Reuse, School of Environment, Key Laboratory of Mesoscopic Chemistry of MOE, School of Chemistry and Chemical Engineering, Nanjing University, Nanjing 210093, P. R. China*

Changjin Tang − *Jiangsu Province Engineering Research Center of Environmental Risk Prevention and Emergency Response Technology, School of Environment, Nanjing Normal University, Nanjing 210023, P. R. China;* orcid.org/0000-0003-0199-0491

Lin Dong − *Jiangsu Key Laboratory of Vehicle Emissions Control, Center of Modern Analysis, State Key Laboratory of Pollution Control and Resource Reuse, School of Environment, Key Laboratory of Mesoscopic Chemistry of MOE, School of Chemistry and Chemical Engineering, Nanjing University, Nanjing 210093, P. R. China;* orcid.org/0000-0002-8393-6669

Complete contact information is available at: https://pubs.acs.org/10.1021/acs.est.4c06313

Notes

The authors declare no competing financial interest.

■ ACKNOWLEDGMENTS

This work was financially supported by the National Natural Science Foundation of China (22202100, 22272077, 62375120, and 22372093) and Natural Science Foundation of Jiangsu Province (BK20231513, BK20240171).

■ REFERENCES

(1) Han, L.; Cai, S.; Gao, M.; Hasegawa, Jy.; Wang, P.; Zhang, J.; Shi, L.; Zhang, D. Selective Catalytic Reduction of NO_x with NH_3 by Using Novel Catalysts: State of the Art and Future Prospects. *Chem. Rev.* **2019**, *119* (19), 10916.

(2) Paolucci, C.; Khurana, I.; Parekh, A. A.; Li, S.; Shih, A. J.; Li, H.; Di Iorio, J. R.; Albarracin-Caballero, J. D.; Yezerets, A.; Miller, J. T.; Delgass, W. N.; Ribeiro, F. H.; Schneider, W. F.; Gounder, R. Dynamic multinuclear sites formed by mobilized copper ions in NO_x selective catalytic reduction. *Science* **2017**, *357* (6354), 898.

(3) Zhang, N.; Li, L.; Guo, Y.; He, J.; Wu, R.; Song, L.; Zhang, G.; Zhao, J.; Wang, D.; He, H. A MnO_2-based catalyst with H_2O resistance for NH_3-SCR: Study of catalytic activity and reactants-H_2O competitive adsorption. *Appl. Catal. B Environ.* **2020**, *270*, No. 118860.

(4) Ji, J.; Gao, N.; Song, W.; Tang, Y.; Cai, Y.; Han, L.; Cheng, L.; Sun, J.; Ma, S.; Chu, Y.; Tang, C.; Dong, L. Understanding the temperature-dependent H_2O promotion effect on SO_2 resistance of MnO_x-CeO_2 catalyst for SCR denitration. *Appl. Catal. B Environ.* **2023**, *324*, No. 122263.

(5) Zhang, G.; Huang, X.; Tang, Z. Enhancing water resistance of a Mn-based catalyst for low temperature selective catalytic reduction reaction by modifying super hydrophobic layers. *ACS Appl. Mater. Interfaces* **2019**, *11* (40), 36598−36606.

(6) Fu, Z.; Zhang, G.; Han, W.; Tang, Z. The water resistance enhanced strategy of Mn based SCR catalyst by construction of TiO_2 shell and superhydrophobic coating. *Chem. Eng. J.* **2021**, *426*, No. 131334.

(7) Bi, F.; Zhang, X.; Chen, J.; Yang, Y.; Wang, Y. Excellent catalytic activity and water resistance of UiO-66-supported highly dispersed Pd nanoparticles for toluene catalytic oxidation. *Appl. Catal. B Environ.* **2020**, *269*, No. 118767.

(8) Wei, Q.; Yu, C.; Song, X.; Zhong, Y.; Ni, L.; Ren, Y.; Guo, W.; Yu, J.; Qiu, J. Recognition of water-induced effects toward enhanced interaction between catalyst and reactant in alcohol oxidation. *J. Am. Chem. Soc.* **2021**, *143* (16), 6071−6078.

(9) An, D.; Ji, J.; Cheng, Q.; Zhao, X.; Cai, Y.; Tan, W.; Tong, Q.; Ma, K.; Zou, W.; Sun, J.; Tang, C.; Dong, L. Facile H_2O-contributed O_2 activation strategy over Mn-Based SCR catalysts to counteract SO_2 poisoning. *Environ. Sci. Technol.* **2023**, *57* (39), 14737−14746.

(10) Wang, C.; Gu, X.-K.; Yan, H.; Lin, Y.; Li, J.; Liu, D.; Li, W.-X.; Lu, J. Water-mediated mars-van krevelen mechanism for CO oxidation on ceria-supported single-atom Pt_1 catalyst. *ACS Catal.* **2017**, *7* (1), 887−891.
(11) Zhao, S.; Chen, F.; Duan, S.; Shao, B.; Li, T.; Tang, H.; Lin, Q.; Zhang, J.; Li, L.; Huang, J.; Bion, N.; Liu, W.; Sun, H.; Wang, A.-Q.; Haruta, M.; Qiao, B.; Li, J.; Liu, J.; Zhang, T. Remarkable active-site dependent H_2O promoting effect in CO oxidation. *Nat. Commun.* **2019**, *10* (1), No. 3824.
(12) Nie, L.; Mei, D.; Xiong, H.; Peng, B.; Ren, Z.; Hernandez, X. I. P.; DeLaRiva, A.; Wang, M.; Engelhard, M. H.; Kovarik, L.; Datye, A. K.; Wang, Y. Activation of surface lattice oxygen in single-atom Pt/CeO_2 for low-temperature CO oxidation. *Science* **2017**, *358* (6369), 1419−1423.
(13) Gu, H.; Lan, J.; Liu, Y.; Ling, C.; Wei, K.; Zhan, G.; Guo, F.; Jia, F.; Ai, Z.; Zhang, L.; Liu, X. Water enables lattice oxygen activation of transition metal oxides for volatile organic compound oxidation. *ACS Catal.* **2022**, *12* (18), 11272−11280.
(14) Xiong, S.; Liao, Y.; Xiao, X.; Dang, H.; Yang, S. Novel effect of H_2O on the low temperature selective catalytic reduction of NO with NH_3 over MnO_x-CeO_2: mechanism and kinetic study. *J. Phys. Chem. C* **2015**, *119* (8), 4180−4187.
(15) Xiong, S.; Liao, Y.; Xiao, X.; Dang, H.; Yang, S. The mechanism of the effect of H_2O on the low temperature selective catalytic reduction of NO with NH_3 over Mn-Fe spinel. *Catal. Sci. Technol.* **2015**, *5* (4), 2132−2140.
(16) Zhang, M.; Gu, K.; Huang, X.; Chen, Y. A DFT study on the effect of oxygen vacancies and H_2O in Mn-MOF-74 on SCR reactions. *Phys. Chem. Chem. Phys.* **2019**, *21*, 19226−19233, DOI: 10.1039/c9cp02640a.
(17) Meng, D.; Xu, Q.; Jiao, Y.; Guo, Y.; Guo, Y.; Wang, L.; Lu, G.; Zhan, W. Spinel structured $Co_aMn_bO_x$ mixed oxide catalyst for the selective catalytic reduction of NO_x with NH_3. *Appl. Catal. B Environ.* **2018**, *221*, 652−663.
(18) Meng, D.; Zhan, W.; Guo, Y.; Guo, Y.; Wang, L.; Lu, G. A Highly Effective Catalyst of Sm-MnO_x for the NH_3-SCR of NO_x at Low Temperature: Promotional Role of Sm and Its Catalytic Performance. *ACS Catal.* **2015**, *5* (10), 5973−5983.
(19) Sun, P.; Long, Y.; Long, Y.; Cao, S.; Weng, X.; Wu, Z. Deactivation effects of Pb(II) and sulfur dioxide on a γ-MnO_2 catalyst for combustion of chlorobenzene. *J. Colloid Interface Sci.* **2020**, *559*, 96−104.
(20) Cheng, S.; Yang, L.; Chen, D.; Ji, X.; Jiang, Z.-J.; Ding, D.; Liu, M. Phase evolution of an alpha MnO_2-based electrode for pseudocapacitors probed by in operando Raman spectroscopy. *Nano Energy* **2014**, *9*, 161−167.
(21) Shan, C.; Zhang, Y.; Zhao, Q.; Fu, K.; Zheng, Y.; Han, R.; Liu, C.; Ji, N.; Wang, W.; Liu, Q. Acid etching-induced in situ growth of λ-MnO_2 over CoMn spinel for low-temperature volatile organic compound oxidation. *Environ. Sci. Technol.* **2022**, *56* (14), 10381−10390.
(22) Li, G.; Li, N.; Sun, Y.; Qu, Y.; Jiang, Z.; Zhao, Z.; Zhang, Z.; Cheng, J.; Hao, Z. Efficient defect engineering in Co-Mn binary oxides for low-temperature propane oxidation. *Appl. Catal. B Environ.* **2021**, *282*, No. 119512.
(23) Mo, S.; Zhang, Q.; Li, J.; Sun, Y.; Ren, Q.; Zou, S.; Zhang, Q.; Lu, J.; Fu, M.; Mo, D.; Wu, J.; Huang, H.; Ye, D. Highly efficient mesoporous MnO_2 catalysts for the total toluene oxidation: Oxygen-Vacancy defect engineering and involved intermediates using in situ DRIFTS. *Appl. Catal. B Environ.* **2020**, *264*, No. 118464.
(24) Liu, Y.; Deng, H.; Lu, Z.; Zhong, X.; Zhu, Y. The study of MnO_2 with different crystalline structures for U(VI) elimination from aqueous solution. *J. Mol. Liq.* **2021**, *335*, No. 116296.
(25) Kang, L.; Zhang, M.; Liu, Z.-H.; Ooi, K. IR spectra of manganese oxides with either layered or tunnel structures. *Spectrochimica Acta A: Molecular Biomolecular Spectroscopy* **2007**, *67* (3), 864−869.
(26) Fink, M. F.; Weiss, M.; Marschall, R.; Roth, C. Experimental correlation of Mn^{3+} cation defects and electrocatalytic activity of α-MnO_2 − an X-ray photoelectron spectroscopy study. *J. Mater. Chem. A* **2022**, *10* (29), 15811−15838.
(27) Fahlman, A.; Hamrin, K.; Hedman, J.; Nordberg, R.; Nordling, C.; Siegbahn, K. Electron spectroscopy and chemical binding. *Nature* **1966**, *210* (5031), 4−8.
(28) Siegbahn, K.; Nordling, C. *ESCA: atomic, molecular and solid state structure studied by means of electron spectroscopy*; Nov. Act. Upsaliensis: Uppsala, 1967.
(29) Lee, S. H.; Rasaiah, J. C. Proton transfer and the mobilities of the H^+ and OH^- ions from studies of a dissociating model for water. *J. Chem. Phys.* **2011**, *135* (12), 124505 DOI: 10.1063/1.3632990.
(30) Gong, P.; Xie, J.; Fang, D.; Han, D.; He, F.; Li, F.; Qi, K. Effects of surface physicochemical properties on NH_3-SCR activity of MnO_2 catalysts with different crystal structures. *Chinese J. Catal.* **2017**, *38* (11), 1925−1934.
(31) Wen, N.; Su, Y.; Deng, W.; Zhou, H.; Hu, M.; Zhao, B. Synergy of CuNiFe-LDH based catalysts for enhancing low-temperature SCR-C_3H_6 performance: Surface properties and reaction mechanism. *Chem. Eng. J.* **2022**, *438*, No. 135570.
(32) Wang, Y.; Chen, L.; Wang, W.; Wang, X.; Li, B.; Zhang, S.; Li, W.; Li, S. Revealing the excellent low-temperature activity of the $Fe_{1-x}Ce_xO_\delta$-S catalyst for NH_3-SCR: Improvement of the lattice oxygen mobility. *ACS Appl. Mater. Interfaces* **2023**, *15* (14), 17834−17847.
(33) Yu, X.; Dai, L.; Deng, J.; Liu, Y.; Jing, L.; Zhang, X.; Gao, R.; Hou, Z.; Wei, L.; Dai, H. An isotopic strategy to investigate the role of water vapor in the oxidation of 1,2-dichloroethane over the Ru/WO_3 or Ru/TiO_2 catalyst. *Appl. Catal. B Environ.* **2022**, *305*, No. 121037.
(34) Hurum, D. C.; Agrios, A. G.; Gray, K. A.; Rajh, T.; Thurnauer, M. C. Explaining the enhanced photocatalytic activity of degussa P25 mixed-phase TiO_2 using EPR. *J. Phys. Chem. B* **2003**, *107* (19), 4545−4549.
(35) Kumar, C. P.; Gopal, N. O.; Wang, T. C.; Wong, M.-S.; Ke, S. C. EPR investigation of TiO_2 nanoparticles with temperature-dependent properties. *J. Phys. Chem. B* **2006**, *110* (11), 5223−5229.
(36) Anpo, M.; Che, M.; Fubini, B.; Garrone, E.; Giamello, E.; Paganini, M. C. Generation of superoxide ions at oxide surfaces. *Top. Catal.* **1999**, *8* (3), 189−198.
(37) Luo, N.; Gao, F.; Liu, H.; Xiong, T.; Wen, J.; Duan, E.; Wang, C.; Zhao, S.; Yi, H.; Tang, X. Hierarchical structured Ti-doped CeO_2 stabilized $CoMn_2O_4$ for enhancing the low-temperature NH_3-SCR performance within highly H_2O and SO_2 resistance. *Appl. Catal. B Environ.* **2024**, *343*, No. 123442.
(38) Zhang, H.; Yang, W.; Roslan, I. I.; Jaenicke, S.; Chuah, G.-K. A combo Zr-HY and Al-HY zeolite catalysts for the one-pot cascade transformation of biomass-derived furfural to γ-valerolactone. *J. Catal.* **2019**, *375*, 56−67.
(39) Wan, Y.; Yang, G.; Xiang, J.; Shen, X.; Du, X. Promoting effect of water on NH_3-SCR reaction over Cu-SAPO-34 catalyst: Transient and permanent influences on Cu species. *Dalton T.* **2019**, *49* (3), 764−773, DOI: 10.1039/c9dt03848e.
(40) Tan, W.; Wang, C.; Yu, S.; Li, Y.; Xie, S.; Gao, F.; Dong, L.; Liu, F. Revealing the effect of paired redox-acid sites on metal oxide catalysts for efficient NO_x removal by NH_3-SCR. *J. Hazard. Mater.* **2021**, *416*, No. 125826.
(41) Ji, J.; Jing, M.; Wang, X.; Tan, W.; Guo, K.; Li, L.; Wang, X.; Song, W.; Cheng, L.; Sun, J.; Song, W.; Tang, C.; Liu, J.; Dong, L. Activating low-temperature NH_3-SCR catalyst by breaking the strong interface between acid and redox sites: A case of model $Ce_2(SO_4)_3$-CeO_2 study. *J. Catal.* **2021**, *399*, 212−223.
(42) Tang, X.; Li, J.; Sun, L.; Hao, J. Origination of N_2O from NO reduction by NH_3 over β-MnO_2 and α-Mn_2O_3. *Appl. Catal. B Environ.* **2010**, *99* (1), 156−162.
(43) Zeng, Y.; Lyu, F.; Wang, Y.; Zhang, S.; Zhong, Q.; Zhong, Z. New insight on N_2O formation over MnO_x/TiO_2 catalysts for selective catalytic reduction of NO_x with NH_3. *Mol. Catal.* **2022**, *525*, No. 112356.

(44) Liu, K.; He, H.; Chu, B. Microkinetic study of NO oxidation, standard and fast NH_3-SCR on $CeWO_x$ at low temperatures. *Chem. Eng. J.* **2021**, *423*, No. 130128.
(45) Huo, Y.; Liu, K.; Liu, J.; He, H. Effects of SO_2 on standard and fast SCR over $CeWO_x$: A quantitative study of the reaction pathway and active sites. *Appl. Catal. B Environ.* **2022**, *301*, No. 120784.
(46) Ji, J.; Tang, Y.; Han, L.; Ran, P.; Song, W.; Cai, Y.; Tan, W.; Sun, J.; Tang, C.; Dong, L. Cerium manganese oxides coupled with ZSM-5: A novel SCR catalyst with superior K resistance. *Chem. Eng. J.* **2022**, *445*, No. 136530.
(47) Tan, W.; Liu, A.; Xie, S.; Yan, Y.; Shaw, T. E.; Pu, Y.; Guo, K.; Li, L.; Yu, S.; Gao, F.; Liu, F.; Dong, L. Ce-Si mixed oxide: A high sulfur resistant catalyst in the NH_3-SCR reaction through the mechanism-enhanced process. *Environ. Sci. Technol.* **2021**, *55* (6), 4017−4026.

https://doi.org/10.1021/acs.est.4c06313
Environ. Sci. Technol. 2024, 58, 16974−16983